High Electron Mobility in [1]Benzothieno[3,2-b][1]benzothiophene-Based Field-Effect Transistors: Toward n-Type BTBTs

Hakan Usta,*,[†] Dojeon Kim,[‡] Resul Ozdemir,[†] Yunus Zorlu,[§] Sanghyo Kim,[∥]
M. Carmen Ruiz Delgado,[⊥] Alexandra Harbuzaru,[⊥] Seonhyoung Kim,[‡] Gökhan Demirel,[#]
Jongin Hong,[‡] Young-Geun Ha,[¶] Kilwon Cho,[∥] Antonio Facchetti,*,[▽,○] and Myung-Gil Kim*,[‡]

[†]Department of Materials Science and Nanotechnology Engineering, Abdullah Gül University, Kayseri 38080, Turkey

[‡]Department of Chemistry, Chung-Ang University, Dongjak-gu, Seoul 06974, Republic of Korea

[§]Department of Chemistry, Gebze Technical University, Gebze 41400, Turkey

[∥]Department of Chemical Engineering, Pohang University of Science and Technology, Pohang 37673, Republic of Korea

[⊥]Department of Physical Chemistry, University of Malaga, Campus de Teatinos s/n, Malaga 29071, Spain

[#]Bio-Inspired Materials Research Laboratory (BIMREL), Department of Chemistry, Gazi University, Ankara 06500, Turkey

[¶]Department of Chemistry, Kyonggi University, Suwon, Gyeonggi-Do 16227, Republic of Korea

[▽]Flexterra Corporation, 8025 Lamon Avenue, Skokie, Illinois 60077-5318, United States

[○]Department of Chemistry and the Materials Research Center, Northwestern University, 2145 Sheridan Road, Evanston, Illinois 60208-3113, USA

S *Supporting Information*

ABSTRACT: The first example of an n-type [1]benzothieno-[3,2-b][1]benzothiophene (BTBT)-based semiconductor, **D-(Ph$_F$CO)-BTBT**, has been realized via a two-step transition-metal-free process without using chromatographic purification. Physicochemical and optoelectronic characterizations of the new semiconductor were performed in detail, and the crystal structure was accessed. The new molecule exhibits a large optical band gap (~2.9 eV) and highly stabilized (ΔE_{LUMO} = 1.54 eV)/π-delocalized lowest unoccupied molecular orbital (LUMO) mainly comprising the BTBT π-core and in-plane carbonyl units. The effect of out-of-plane twisted (64°) pentafluorophenyl groups on LUMO stabilization is found to be minimal. Polycrystalline **D(Ph$_F$CO)-BTBT** thin films prepared by physical vapor deposition exhibited large grains (~2−5 μm sizes) and "layer-by-layer" stacked edge-on oriented molecules with an in-plane herringbone packing (intermolecular distances ~3.25−3.46 Å) to favor two-dimensional (2D) source-to-drain (S → D) charge transport. The corresponding TC/BG-OFET devices demonstrated high electron mobilities of up to ~0.6 cm^2/V·s and I_{on}/I_{off} ratios over 10^7−10^8. These results demonstrate that the large band gap BTBT π-core is a promising candidate for high-mobility n-type organic semiconductors and, combination of very large intrinsic charge transport capabilities and optical transparency, may open a new perspective for next-generation unconventional (opto)electronics.
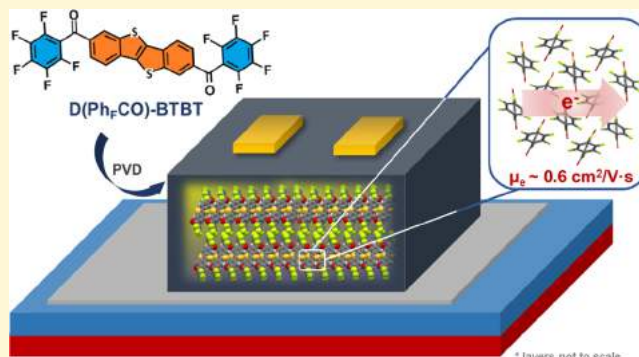
INTRODUCTION

The development of π-conjugated small-molecule semi-conducting materials is an emerging and continuously growing research area in organic (opto)electronics.[1−5] Semiconducting small molecules are the key active layer component of high-performance organic field-effect transistors (OFETs) used for the next-generation (opto)electronic technologies such as logic circuits on plastic substrates, flexible displays, and electronic skins.[6−10] The main motivations for continuously designing and synthesizing new π-conjugated frameworks in the past few decades do not only include improving charge transport

characteristics and realizing novel functions but also to better understand and address fundamental structure-(opto)-electronic property—electrical performance relationships.[11−16] Since the initial report of small-molecule-based OFETs three decades ago,[17] the search for semiconducting small molecules has primarily focused on fused (hetero)acene structures including [1]benzothieno[3,2-b][1]benzothiophene (BTBT)
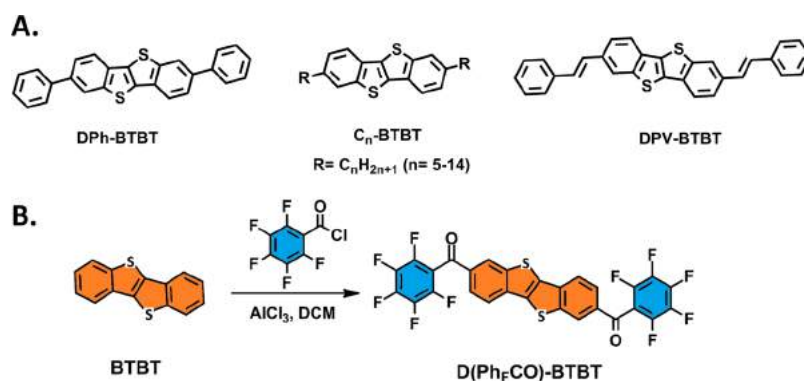
Figure 1. (A) Chemical structures of BTBT-based p-type molecular semiconductors **DPh-BTBT**, **C$_n$-BTBT**, and **DPV-BTBT** reported in the literature.[24−26] (B) Synthesis of the current n-type semiconductor **D(Ph$_F$CO)-BTBT**.

derivatives.[18−20] The synthesis of BTBT π-core was first conveyed in 1950s,[21] and the earlier derivatives were studied as liquid crystals.[22,23] The semiconducting properties of this family were unexplored until the pioneering studies by Takimiya et al., which demonstrated p-type charge transport for vapor-deposited films of 2,7-diphenylbenzo[b]benzo[4,5]-thieno[2,3-d]thiophene (**DPh-BTBT**) and spin-coated films of 2,7-dialkyl[1]benzothieno[3,2-b][1]benzothiophene (**C$_n$-BTBT**, n = 5−14) (Figure 1A).[24,25] Following these studies, numerous functionalized BTBT derivatives (Figure S1) have been developed for use in OFETs, including additional core functionalization and core extension by benzofusion.[24−33] Furthermore, the crystallinity/packing properties of the well-known derivative **C$_8$-BTBT** (n = 8) have been tuned via unconventional solution-based film fabrication techniques (i.e., antisolvent-assisted inkjet printing and off-center spin-coating), yielding impressive charge transport characteristics.[34,35]

There are several reasons for the incredibly rapid emergence of BTBT-based semiconducting molecules in the past decade: (i) facile π-core synthesis and functionalization allowing fine tuning of solid-state packing, solubility, and frontier orbital properties; (ii) the presence of a fused rigid π-system with structural symmetry and high coplanarity, which facilitates charge carrier delocalization and intermolecular interactions; (iii) large frontier orbital coefficients on the sulfur atoms, which is beneficial for effective intermolecular orbital overlap and large transfer integrals;[36] (iv) the presence of thieno[3,2-b]thiophene unit in the center of a thienoacene π-framework and phene-type π-electronic structure resulting in large optical band gap (>3.0 eV) and stabilized highest occupied molecular orbital (HOMO) energy level (<−5.5 eV).[36−38] Despite these very attractive structural/electronic properties and great progresses shown until today, all reported BTBT derivatives are hole-transporting (p-type) semiconductors. To the best of our knowledge, an n-type (electron-transporting) BTBT semiconductor is currently unknown in the literature and the fundamentals remain to be established. This is most likely the result of very high lowest unoccupied molecular orbital (LUMO) energy level and large band gap of fused π-core in BTBT ($E_{g(opt)}$ = 3.65 eV, E_{LUMO} = −2.10 eV in **C$_8$-BTBT**)[25] as compared with those of similar sized nonfused π-systems such as quaterthiophene (E_g = 2.89 eV, E_{LUMO} = −2.90 eV)[39,40] and hexyl-substituted bis(phenyl)-bithiophene (E_g = 2.97 eV).[41] The only known example of the electron-transporting BTBT-based material involves a single-crystalline donor−acceptor mixture of the p-type **C$_n$-BTBT** donor with an n-type tetracyanoquinodimethane acceptor.[42] This arises an impor-

tant question whether BTBT, as a wide band gap π-core, would ever allow energetically stabilized (<−3.0 eV) LUMO and good electron-injection/transport characteristics. Toward this end, we focus on symmetric functionalization of the BTBT π-core in the molecular long-axis direction with pentafluorophenylcarbonyl (Ph$_F$CO) groups. The strong electron-withdrawing characteristics of the combined pentafluorophenyl (Ph$_F$) and carbonyl (C=O) units are envisioned to lower frontier orbital energies, extend π-conjugation, and facilitate electron injection/delocalization on the molecular π-backbone.[43,44] In addition, as a result of the presence of these groups along long axis at the molecular termini, lateral noncovalent interactions between the BTBT π-cores should still be effective for efficient charge transport.

We present herein the design, synthesis, and full characterization of a new BTBT-based semiconducting small molecule, **D(Ph$_F$CO)-BTBT**, which was developed via a two-step transition-metal-free process without using chromatographic purification. Physicochemical and optoelectronic characterizations of the new semiconductor were performed in detail, and the crystal structure was accessed. The new molecule exhibits a large optical band gap (~2.9 eV) and highly stabilized (−3.64 eV)/π-delocalized LUMO mainly comprising the BTBT π-core and in-plane carbonyl units. The effect of out-of-plane twisted (64°) pentafluorophenyl groups on LUMO stabilization is found to be minimal. Polycrystalline **D(Ph$_F$CO)-BTBT** thin films prepared by physical vapor deposition (PVD) exhibit large grains (~2−5 μm sizes) and "layer-by-layer" stacked edge-on oriented molecules with an in-plane herringbone packing (intermolecular distances ≈ 3.25−3.46 Å). The new molecule exhibits an n-type semiconductor behavior in OFETs with a high electron mobility (μ_e) of 0.57 cm^2/V·s and current modulation (I_{on}/I_{off}) over 10^7 to 10^8. **D(Ph$_F$CO)-BTBT** is demonstrated to be the first n-type BTBT semiconductor, which could open new possibilities for future complementary optical and circuitry applications.

■ EXPERIMENTAL SECTION

Materials and Methods. Unless otherwise noted, all reagents were purchased from commercial sources and used without further purification. All nonaqueous reactions were carried out in a dried glassware under an inert atmosphere of N$_2$. ^{1}H NMR spectroscopy characterizations were performed by using a Bruker 400 spectrometer (^{1}H at 400 MHz). Elemental analyses were recorded on a LecoTruspec Micro model instrument. The intensity data for **D(Ph$_F$CO)-BTBT** single crystal were collected on a Bruker APEX II QUAZAR three-circle diffractometer using monochromatized Mo

Kα X-radiation (λ = 0.71073 Å). Single-crystal structure refinement was performed as explained in the Supporting Information. Thermal characterizations of thermogravimetric analysis (TGA) and differential scanning calorimetry (DSC) were performed under nitrogen at a heating rate of 10 °C/min using PerkinElmer Diamond model instruments. Cyclic voltammetry measurements were carried out using a BASi-Epsilon potentiostat/galvanostat from Bioanalytical Systems Inc. (Lafayette, IN) equipped with a C3-cell stand electrochemical station. Working and counter electrodes were Pt, and the reference electrode was Ag/AgCl (3 M NaCl). All potentials were calibrated with a standard ferrocene/ferrocenium redox couple (Fc/Fc$^+$: $E_{1/2}$ = +0.40 V measured in the current electrochemical setup). High-resolution mass spectra were measured on a Bruker Microflex LT MALDI-TOF-MS. UV−vis absorption spectra were recorded by using a Shimadzu UV-1800 spectrophotometer. The optimization of the molecular geometries and analysis of frontier molecular orbitals were carried out with Gaussian 09 by using DFT at B3LYP/6-31G** level.[45]

Field-Effect Transistor Fabrication and Characterization. A heavily n-doped (100) silicon substrate (gate) with 200 nm thermally grown SiO$_2$ (gate dielectric) was used as the semiconductor thin-film platform. The substrates were sonicated in isopropyl alcohol for 10 min with subsequent drying under N$_2$ flow, which was followed by 100 W oxygen plasma treatment for 3 min (Cute, Femto Science, South Korea). The hydrophobic surface was obtained with hexamethyldisilazane (HMDS) vapor treatment on 200 nm SiO$_2$/n^{++}Si. The 30 nm **D(Ph$_F$CO)-BTBT** thin films were grown via thermal evaporation on O$_2$ plasma-treated n^{++}-Si/SiO$_2$(200 nm) and n^{++}-Si/SiO$_2$(200 nm)/HMDS substrates under high vacuum (∼10^{-6} Torr) at various substrate temperatures (25, 70, 100, and 120 °C) using a growth rate of 0.1−0.2 Å/s. To complete the field-effect transistor device architecture, LiF (1 nm)/Au (50 nm) or Au (50 nm) source−drain electrodes were thermally evaporated through a shadow mask to define 50 μm semiconductor channel length and 1000 μm semiconductor channel width. The surface morphology and microstructure of the semiconductor thin films were characterized by atomic force microscopy (AFM, NX10, Park systems) and grazing incidence X-ray diffraction (GIXD, PLS-II 9A U-SAXS beamline of Pohang Accelerator Laboratory in Korea) techniques, respectively. The electrical characteristics of the **D(Ph$_F$CO)-BTBT**-based field-effect transistor devices in top-contract/bottom-gate geometries were analyzed by using a vacuum probe station (M5VC, MSTech, South Korea) and Keithley 4200-SCS semiconductor analyzer system (Tektronix Inc, USA). The saturation charge carrier mobility (μ_{sat}) for each device fabrication condition was calculated as the average value of at least 10 OFET devices using the formula

$$\mu_{sat} = (2I_{DS}L)/[WC_i(V_G - V_{th})^2]$$

where I_{DS} is the source−drain current, L is the channel length, W is the channel width, C_i is the areal capacitance of the gate dielectric, V_G is the gate voltage, and V_{th} is the threshold voltage. The voltage ranges used in charge carrier mobility calculations are between 50 and 80 V.

Synthesis and Characterization. BTBT and the reference compounds D(C$_7$CO)-BTBT and C$_8$-BTBT were prepared in accordance with the reported procedure.[23,25]

Caution: 2,3,4,5,6-Pentafluorobenzoyl chloride and aluminum chloride (AlCl$_3$) react violently with water and should be handled with great care.

Synthesis of benzo[b]benzo[4,5]thieno[2,3-d]thiophene-2,7-diylbis-((perfluorophenyl) methanone) (D(Ph$_F$CO)-BTBT): aluminum chloride (AlCl$_3$) (3.05 g, 22.88 mmol) was added into a solution of BTBT (1.0 g, 4.16 mmol) in dichloromethane (100 mL) at −10 °C under nitrogen. The resulting reaction mixture was stirred at −10 °C for 30 min. Then, 2,3,4,5,6-pentafluorobenzoyl chloride (3.7 mL, 25.8 mmol) was added dropwise, and the mixture was stirred for 1 h at the same temperature. The reaction mixture was allowed to warm to room temperature and stirred for 2 days. The reaction mixture was quenched with water to give a pale yellow precipitate. The precipitate was collected by filtration, and washed with water and methanol in

sequence. Because of its limited solubility in common organic solvents, the crude was purified by thermal gradient sublimation under high vacuum ($P \approx 1 \times 10^{-5}$ Torr). The product was obtained as a light yellow solid (0.54 g, 21% yield). Melting point: 336−337 °C; ^{1}H NMR (400 Mhz, CDCl$_3$): δ (ppm) 8.46 (s, 2H), 8.07 (d, J = 8.0 Hz, 2H), 7.99 (d, J = 8.0 Hz, 2H); MS (MALDI-TOF) m/z [M$^+$]: calcd for C$_{28}$H$_6$F$_{10}$O$_2$S$_2$, 627.96; found, 627.90. Elemental analysis (%) calcd for C$_{28}$H$_6$F$_{10}$O$_2$S$_2$: C, 53.51; H, 0.96; found: C, 53.36; H, 0.99.

Theoretical Methodology. The intramolecular reorganization energies associated with hole (λ_h) and electron transfer (λ_e) were calculated for **C$_8$-BTBT** and **D(Ph$_F$CO)-BTBT**, respectively, using a standard procedure reported in the literature.[46] The transfer integrals for electrons (t_e) in **D(Ph$_F$CO)-BTBT** dimers within the herringbone-layered structure were calculated by using the approach described by Valeev et al.[47] with the corresponding matrix elements evaluated with Gaussian 09.[45] For comparison purposes, the transfer integrals for holes (t_h) in **C$_8$-BTBT** dimers within the herringbone-layered structure were also calculated. The B3LYP[48,49] and PW91PW91[50,51] functionals are considered together with the 6-31G** basis set.[52,53] Note that the electronic coupling value is dependent on the functional employed in the calculation, and it generally increases with the percentage of Hartree−Fock exchange.[54] The transfer integrals calculated with the B3LYP exchange−correlation functional give very trends similar to those obtained using PW91PW91 (Tables S3 and S4).

RESULTS AND DISCUSSION

Theoretical Calculations, Synthesis, and Characterization. Prior to the synthesis of the new small molecule, electronic/structural effects of pentafluorophenylcarbonyl functionalization on the wide band gap BTBT core were studied via DFT (B3LYP/6-31G**) computations. Among the four possible positions on the outer benzene rings of BTBT, functionalization at 2,7-positions is found to provide the lowest LUMO energy level with the greatest wave function delocalization (Figure S2). DFT calculations also show that the "CO−BTBT−CO" π-segment adopts a good coplanarity with small torsional angles ($\theta_{C=C−C=O}$ < 5°) between the carbonyl and the BTBT units (Figure S3). On the other hand, the pentaflurophenyl groups, as expected based on the crystal structures of previously developed Ph$_F$CO-functionalized arenes,[44,55,56] adopt highly twisted conformations with respect to this coplanar π-segment with a dihedral angle of 64.1°. These structural features at the molecular level lead to a unique electronic structure in **D(Ph$_F$CO)-BTBT** showing energetically stabilized frontier orbitals (ΔE_{HOMO} = −0.88 eV and ΔE_{LUMO} = −1.70) and significantly reduced HOMO−LUMO gap (ΔE = −0.82 eV) compared to the parent p-type semiconductor **C$_8$-BTBT** (Figure S3). The LUMO shows a significant contribution from carbonyl groups, whereas the HOMO remains mostly localized on the central BTBT π-unit, which explains the much higher energetic stabilization of the LUMO versus the HOMO. Interestingly, the pentafluorophenyl terminal units do not participate in both frontier orbitals as a result of the large torsion; therefore, they are involved in the electronic stabilization of the molecular orbitals solely via a negative inductive ($-I$) effect on the π-system. On the other hand, the highly coplanar carbonyl units exhibit considerable negative resonance ($-R$) effect on the π-electron system. This result is consistent with the fact that they constitute a crucial part of the LUMO topology. The single-crystal structure and experimental frontier orbital energies are found to closely match the theoretical structural and electronic findings (vide infra).
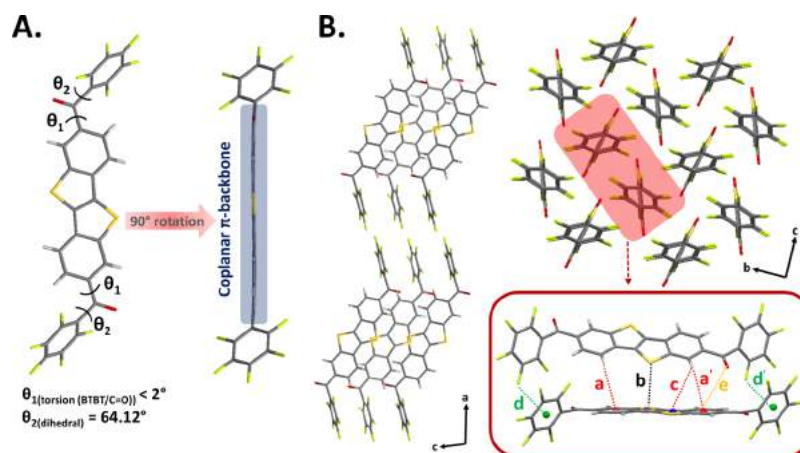
Figure 2. (A) Capped-stick drawings of the crystal structure of **D(Ph$_F$CO)-BTBT** showing the corresponding dihedral and torsion angles and π-backbone coplanarity. (B) Perspective views of the molecular arrangements along the a,c-axes and b,c-axes showing the alternately stacked layers and the 2D herringbone-like packing, respectively. The inset shows the pairs of **D(Ph$_F$CO)-BTBT** molecules in the herringbone motif with CH···π (benzene/thiophene) (a = 3.45 Å; a' = 3.25 Å/c = 3.46 Å), S···π (thiophene) (b = 3.38 Å), F···π (pentafluorobenzene) (d = 3.30 Å; d' = 3.16 Å), and O···π (benzene) (d = 3.52 Å) contacts.

D(Ph$_F$CO)-BTBT was synthesized in 45% yield via double Friedel−Crafts acylation at the 2,7-positions of the BTBT (Figure 1B) and purified by thermal gradient sublimation under high vacuum (1×10^{-5} Torr). The chemical structure and purity of **D(Ph$_F$CO)-BTBT** were characterized and established by nuclear magnetic resonance (NMR) spectroscopy (Figure S4), elemental analysis, mass spectrometry (Figure S5), and single-crystal X-ray diffraction. From a materials production standpoint, it is quite promising that the new semiconductor could be synthesized in a two-step transition-metal-free process without using chromatographic purification. Although **D(Ph$_F$CO)-BTBT** solubility in common organic solvents at room temperature is quite low, the ^{1}H NMR spectrum recorded at an elevated temperature in CDCl$_3$ revealed that the chemical shifts of the aromatic protons in **D(Ph$_F$CO)-BTBT** moved downfield ($\Delta\delta \approx 0.7-0.8$ ppm) with respect to those in **C$_8$-BTBT** (δ_{Ar-H} = 7.2−7.8 ppm → 8.0−8.5 ppm). This indicates substantially reduced electron density (deshielding effect) on the BTBT π-system because of the presence of strongly electron-withdrawing pentafluorophenylcarbonyl (Ph$_F$CO) end-units. TGA at reduced pressure (∼0.1 Torr) shows very clean, quantitative sublimation with good thermal robustness for the new **D(Ph$_F$CO)-BTBT** π-framework (Figure S6A). This is undoubtedly the result of arene-fluorination at the molecular termini that provides excellent volatility for the reliable and quantitative film fabrication via PVD. The DSC measurement shows endothermic (+146.7 J/g) and exothermic (−103.47 J/g) thermal transitions at 338 and 301 °C, respectively (Figure S6B). Conventional melting point measurement shows that these transitions correspond to melting (mp 336−337 °C) and crystallization processes, respectively. No evidence of mesophase formation was observed before melting, which is consistent with the previously reported pentafluorophenyl-substituted molecular semiconductors.[44,57]

Single-Crystal Structure Analysis. Light yellow crystals of **D(Ph$_F$CO)-BTBT** suitable for X-ray diffraction (Figure 2) were grown by thermal gradient sublimation. This molecule crystallizes in the monoclinic space group $C2/c$ showing a "layer-by-layer" packing motif along the crystallographic a-axis consisting of alternately stacked "CO−BTBT−CO" and

"pentafluorophenyl" layers (Figure 2B). These layers are extended into the b- and c-axes to form a typical herringbone-like molecular packing, which could facilitate two-dimensional (2D) charge transport. The major intermolecular interactions governing the herringbone motif are identified as CH···π (benzene/thiophene) (a = 3.45 Å; a' = 3.25 Å/c = 3.46 Å), S···π (thiophene) (b = 3.38 Å), F···π (pentafluorobenzene) (d = 3.30 Å/d' = 3.16 Å), and O···π (benzene) (d = 3.52 Å) contacts (Figure 2B). In addition, short S···S (3.38 Å < r_{vdw}(S) + r_{vdw}(S) = 3.60 Å) contacts also exist between the thiophene rings along the c-axis. As shown in Figure 2A, the "CO−BTBT−CO" π-segment exhibits a substantially coplanar backbone with the carbonyl units lying perfectly in the plane; the torsion angle for C8−C7−C═O is only −1.9(4)°. The dihedral angle between pentafluorophenyl ring and the BTBT core is measured to be ∼64.12°. The observed solid-state conformation is consistent with the DFT-calculated molecular structure (vide supra), and it yields extended π-conjugation along the molecular backbone including the BTBT and the carbonyl units.

Optical and Electrochemical Properties. The UV−vis absorption spectrum and cyclic voltammogram of **D(Ph$_F$CO)-BTBT**, along with the reference molecule **C$_8$-BTBT**, were recorded in a dichloromethane solution to assess the effects of carbonyl and pentafluorophenyl substitutions on BTBT core optical absorption and the frontier orbital energies. As shown in Figure 3A, **D(Ph$_F$CO)-BTBT** exhibits typical vibronic features of a fused heteroacene π-system with substantially red-shifted ($\Delta\lambda \approx 90-100$ nm) low-energy absorption maximum (λ_{max} = 406 nm) and onset (λ_{onset} = 435 nm) values as compared with **C$_8$-BTBT**. The optical band gap for **D(Ph$_F$CO)-BTBT** is estimated as 2.85 eV, which is considerably smaller ($\Delta E_{g(opt)}$ = −0.80 eV) than that of **C$_8$-BTBT** ($E_{g(opt)}$ = 3.65 eV). When going from solution to a vapor-deposited thin film, **D(Ph$_F$CO)-BTBT** exhibits a new low-energy absorption maximum at 429 nm with an onset at 453 nm ($E_{g(opt-film)}$ = 2.75 eV), indicating intermolecular interactions in the solid state (Figure S7). When compared with typical n-type semiconductors reported in the literature ($E_{g(opt)}$ = 1.3−2.5 eV),[58] the relatively large solid-state optical band gap of **D(Ph$_F$CO)-BTBT**, resulting in excellent trans-
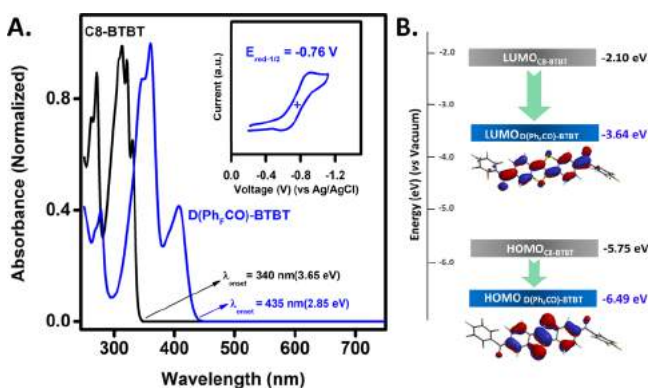
Figure 3. (A) Optical absorption spectra of **D(Ph$_F$CO)-BTBT** and the reference molecule **C$_8$-BTBT** in dichloromethane solutions, and cyclic voltammogram (inset) for **D(Ph$_F$CO)-BTBT** in dichloromethane (0.1 M Bu$_4$N$^+$PF$_6^-$, scan rate = 50 mV s^{-1}). (B) Experimental HOMO/LUMO energy levels for **D(Ph$_F$CO)-BTBT** and **C$_8$-BTBT** and topographical orbital representations (DFT/B3LYP/6-31G**) for **D(Ph$_F$CO)-BTBT**.

parency in the visible region (Figure S8), could be advantageous for carbon-based transparent electronics and multilayer green/blue-emitting transistors (OLETs).[59,60] In contrast to the electrochemical behavior of p-type **C$_8$-BTBT** that only shows an oxidation peak at +0.89 V (vs Fc/Fc$^+$),[25] **D(Ph$_F$CO)-BTBT** exhibits a quasi-reversible reduction peak with the half-wave reduction potential at −0.76 V (vs Ag/AgCl). The LUMO and HOMO energies of the new molecule are estimated as −3.64 and −6.49 eV (Figure 3B), respectively, which are far lower than those of **C$_8$-BTBT** (E_{LUMO} = −2.10 eV and E_{HOMO} = −5.75 eV) measured in the same electrochemical setup (Figure S9). Going from **C$_8$-BTBT** to **D(Ph$_F$CO)-BTBT**, the occurrence of an electrochemical reduction process, E_{LUMO}/E_{HOMO} stabilizations (noting with a much larger degree for the former orbital), and the reduction in the optical band gap are all in good agreement with the DFT calculations. This clearly points to the efficient electron-withdrawing capacities of the combined carbonyl and pentafluorophenyl units, which could induce electron transport in semiconductor devices. Note that the LUMO energy level for **D(C$_7$CO)-BTBT**, which is a BTBT derivative with the combined electron-donating heptyl (−C$_7$H$_{15}$) and the electron-withdrawing carbonyl units, is already at −3.54 eV (Figure S10). Thus, it is clear that major LUMO stabilization for **D(Ph$_F$CO)-BTBT** (∼1.44 eV) originates from the presence of the in-plane oriented carbonyl functionalities [negative resonance (−R) effect], whereas the out-of-plane twisted pentafluorophenyl units provide minimal stabilization (∼0.1 eV) via a negative inductive (−I) effect. Similar LUMO stabilization trends were previously observed in pentafluorophenyl- versus phenyl-substituted dicarbonyl oligothiophenes.[44] It is also noteworthy that (partial) fluorination of semiconducting cores can favorably affect electron transport by acting as a kinetic barrier to adsorption of components (i.e., H$_2$O/O$_2$) acting as charge traps.[43,61,62]

Thin-Film Microstructure/Morphology and Field-Effect Transistor Characterization. Charge transport characteristics of the new semiconductor were investigated in top-contact bottom-gate (TC/BG) OFETs, which were fabricated by vapor deposition of **D(Ph$_F$CO)-BTBT** thin films (∼30 nm) onto temperature-controlled n^{++}-Si/SiO$_2$(200 nm) and n^{++}-Si/SiO$_2$(200 nm)/HMDS substrates under high

vacuum (∼10^{-6} Torr), followed by Au (50 nm), LiF/Au (1 nm/50 nm), Ag (50 nm), or Al (50 nm) thermal evaporation to define source-drain electrodes and the semiconductor channel [1000 μm (W) × 50 μm (L)]. During the semiconductor film deposition, the substrate temperature was maintained at 25, 70, 100, and 120 °C. Before charge transport measurements, the morphology and microstructure of all of the **D(Ph$_F$CO)-BTBT** films were explored by 2D-GIXD and AFM, which clearly reveals that **D(Ph$_F$CO)-BTBT** adopts an edge-on molecular orientation on the substrate surface forming 2D plate-like grains of terraced islands along the substrate plane (Figures 4C, and S11−S14). The strong diffractions observed by 2D-GIXD analysis correlate perfectly with the single-crystal phases; although (200), (400), and (600) planes are identified in the out-of-plane direction, (020), (111), and (002) planes are identified as the major diffractions in the in-plane direction. This result indicates the formation of edge-on molecular packing motif in the crystalline domains, in which the "CO−BTBT−CO" π-frameworks are tilted at ∼35° from the substrate normal forming a herringbone packing with favorable intermolecular distances (3.25−3.46 Å) along the charge-transport direction (Figure 4D). The BFDH (Bravais−Friedel−Donnay−Harker) theoretical crystal morphology further confirms the formation of plate-like grains on the substrate surface, which extends its 2D crystal plane along the
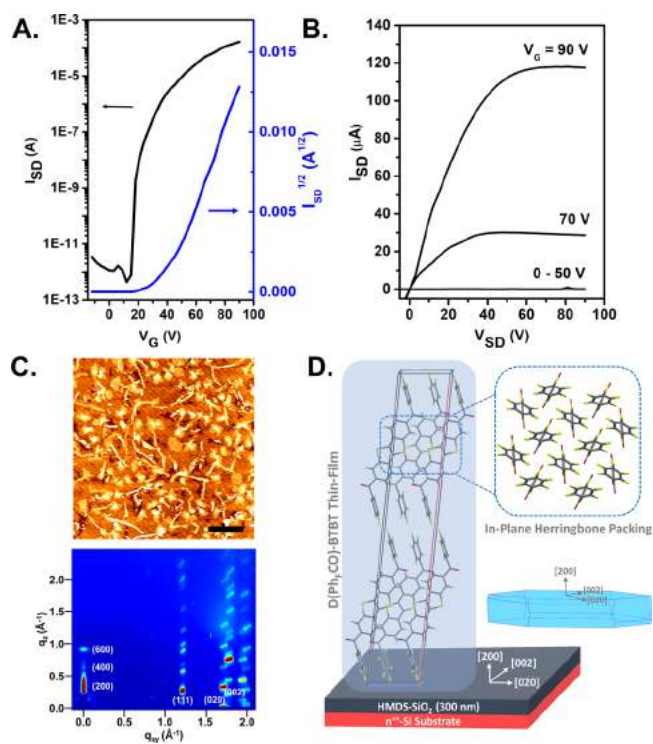

Figure 4. (A) Transfer (V_{SD} = 100 V) and (B) output characteristics for the n^{++}-Si/SiO$_2$(200 nm)/HMDS/**D(Ph$_F$CO)-BTBT**(30 nm)/LiF (1 nm)-Au (50 nm) OFET device. (C) Tapping mode AFM topographic image and 2D-GIXD patterns for **D(Ph$_F$CO)-BTBT** thin films (30 nm) vapor-deposited at 100 °C on n^{++}-Si/SiO$_2$(200 nm)/HMDS. The scale bar denotes 2 μm. (D) Views of the packing arrangement in the **D(Ph$_F$CO)-BTBT** semiconductor layer showing the edge-on molecular orientation (out-of-plane) and the herringbone packing motif (in-plane). The inset shows the BFDH (Bravais, Friedel, Donnay and Harker) theoretical crystal morphology and the corresponding crystallographic directions.
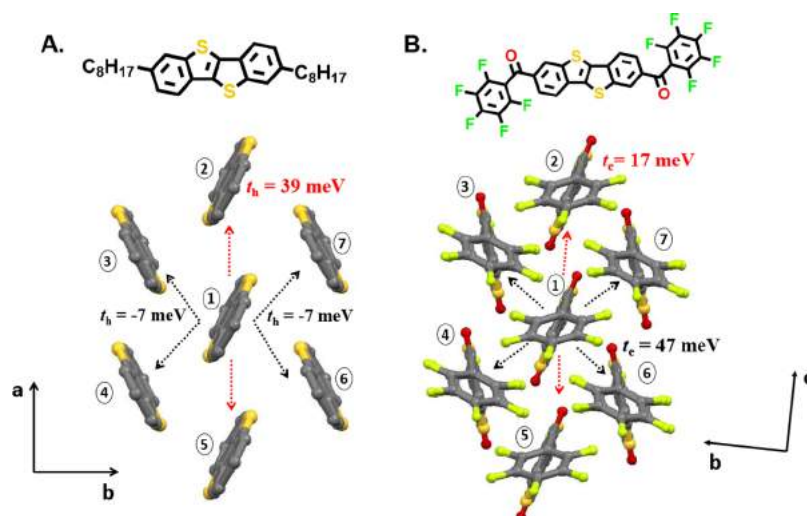
Figure 5. Crystal structures of **C$_8$-BTBT** (A) and **D(Ph$_F$CO)-BTBT** (B) along the *a,b*-axes and *b,c*-axes, respectively, underscoring the formation of 2D in-plane herringbone-like packing. Alkyl chains of **C$_8$-BTBT** are omitted for clarity. DFT estimates of the effective transfer integrals (in meV) for holes (t_h) and electrons (t_e) for the selected dimer pairs in face-to-edge (black dotted lines) and edge-to-edge manners (red dotted lines) are also shown.

(200) plane via herringbone packing (Figure 4D-inset). The step heights (~2.4−2.6 nm, Figure S14) along terraced islands match well with this model corresponding to the half of the unit cell parameter along the *a*-axis and the **D(Ph$_F$CO)-BTBT**'s molecular size (~2.2 nm). Note, **D(Ph$_F$CO)-BTBT** films grown on HMDS-treated Si/SiO$_2$ substrates exhibit, compared with those deposited on the bare SiO$_2$ surface, larger crystallites (Figure S11) as a result of low surface energy better matching with the hydrophobic nature of the fluorinated semiconductor.[63,64] The 2D-GIXD measurements also reveal the effect of surface hydrophobicity on **D(Ph$_F$CO)-BTBT** thin-film growth. As shown in Figure S13, although the room-temperature deposited semiconductor film on the bare SiO$_2$ surface shows ring patterns, indicating misaligned crystalline domains, the room-temperature deposited films on the HMDS-treated surface show phase-pure crystalline domains. Additionally, the semiconductor grain size is found to continuously increase with increasing the substrate temperature (25 °C → 100 °C) from 100−200 nm to ~0.5−1.0 μm on the base SiO$_2$ surfaces and from 300−500 nm to ~2−5 μm on the HMDS-treated substrates (Figure S11).

The electrical characteristics of the **D(Ph$_F$CO)-BTBT**-based OFET devices were measured under positive and negative gate biases to explore the majority charge carrier type and evaluate the semiconductor performance. Considering that the LUMO level (−3.64 eV) for the new semiconductor is higher than those of typical air-stable n-type semiconductors (<~−4 eV),[2,19] our OFETs were tested under an inert (vacuum) atmosphere. Representative transfer/output plots are shown in Figures 4A,B, S15, and S16, whereas the OFET data are summarized in Table S2. All devices, regardless of the SiO$_2$ functionalization and substrate temperatures (T_D), exhibit n-channel behaviors with excellent current modulation characteristics. To the best of our knowledge, **D(Ph$_F$CO)-BTBT** is the first example of a BTBT-based electron-transporting organic semiconductor.

The room-temperature deposited OFET devices with Au (ϕ = 5.1 eV) S−D electrodes on bare and HMDS-treated SiO$_2$ exhibit μ_e's of 0.18 cm^2/V·s (V_{th} = +40.9 V) and 0.14 cm^2/V·s (V_{th} = +39.0 V), respectively, with I_{on}/I_{off}'s of 10^7−10^8. In order to improve electron injection into the **D(Ph$_F$CO)-BTBT** semiconductor channel, lower work function metals [i.e., Ag (ϕ = 4.6 eV) or Al (ϕ = 4.1 eV)] and modified gold [i.e., LiF/Au (ϕ = 3.6 eV)] source−drain electrodes were used as they better match with the LUMO level (−3.64 eV) of the new semiconductor.[65,66] Although OFETs with Ag showed a reduced V_{th} of +29.0 V, the use of both Ag and Al electrodes deteriorated device performances (Table S2 and Figure S17) probably because of unfavorable metal/semiconductor contacts resulting in poor electron injection.[67] On the other hand, the devices with LiF/Au electrodes, which has the closest electrode/semiconductor-LUMO energy match, exhibited the best performance (μ_e of 0.12 cm^2/V·s and I_{on}/I_{off} = 2 × 10^6) with a reduced V_{th} of +31.6 V.[68] For OFETs with LiF/Au electrodes, further improvement in the semiconducting characteristics was achieved by increasing T_D to 70 and 100 °C, which results in μ_e's of 0.45 cm^2/V·s (V_{th} = +37.5 V) and 0.57 cm^2/V·s (V_{th} = +41.8 V), respectively (I_{on}/I_{off}'s ≈ 10^7 to 10^8). The enhanced device characteristics measured at higher deposition temperatures are consistent with the improved morphological/microstructural features (larger crystalline grains and improved edge-on orientation) observed at these deposition temperatures (vide supra). However, further increase of T_D to 120 °C degrades electron transport [μ_e = 0.08 cm^2/V·s, V_{th} = +47.4 V, I_{on}/I_{off} ≈ 10^6]. The deteriorated performance is attributed to partial re-evaporation of **D-(Ph$_F$CO)-BTBT** molecules at higher temperatures, resulting in poor intergrain connectivity (Figure S12). As expected, semiconductor depositions at higher substrate temperatures (T_D > 130 °C) did not yield any semiconductor film formation on the substrate. Although **D(Ph$_F$CO)-BTBT** demonstrates the first n-type BTBT-based semiconductor with a high electron mobility, one should note that the LUMO level is well above the ambient stability threshold (~−4 eV) and the work functions of typical stable electrodes (~5 eV). This not only precludes thermodynamic ambient stability during transistor operation but also introduces injection barriers at the metal/ **D(Ph$_F$CO)-BTBT** contacts. Although LiF/Au seemed to address the latter issue partially, we note that further enhancement of electron injection into the **D(Ph$_F$CO)-**

BTBT thin film by using different electrodes/interlayers could lead to additional improvements in the corresponding n-channel OFET performance.[67] For ambient-stable electron transport, we note that chemical functionalizations on the dicarbonyl BTBT π-system with much stronger electron-withdrawing substituents (e.g., −CN, C=C(CN)$_2$, and C=S) would be necessary to further lower the frontier orbital energetics.[69] However, **D(Ph$_F$CO)-BTBT**-based OFETs could operate with proper encapsulations, which is no matter needed when these TFTs drive, for instance, an OLED device.[70,71] In addition, thanks to **D(Ph$_F$CO)-BTBT**'s high electron mobility, HOMO/LUMO energy levels, wide optical band gap, and smooth 2D film-forming ability via vapor deposition, it could find applications as an electron-transporting/hole-blocking interlayer in (encapsulated) multilayer (opto)electronic devices such as OLETs.[60,72]

In order to elucidate the observed high electron mobility of **D(Ph$_F$CO)-BTBT** in comparison to the benchmark p-type analogue **C$_8$-BTBT**, two important molecular charge transport parameters were studied via DFT calculations: (i) intra-molecular reorganization energy (λ) and (ii) effective transfer integral (t). Although the intramolecular reorganization energy ($\lambda_{h/e}$) characterizes the structural reorganization needed to accommodate a hole/electron, respectively, the effective transfer integral ($t_{h/e}$) reflects the degree of intermolecular electronic interactions for hole/electron transfer between nearest-neighbor molecular pairs. From a molecular level charge transport perspective, a smaller $\lambda_{h/e}$ and larger $t_{h/e}$ values typically lead to high mobility for the corresponding charge carrier type. The reorganization energy associated with the electron transfer (λ_e) for **D(Ph$_F$CO)-BTBT** is calculated to be 315 meV, which is slightly larger than that associated with the hole transfer (λ_h) of the reference molecule **C$_8$-BTBT** (243 meV). However, the calculated λ_e value for **D(Ph$_F$CO)-BTBT** is in the same range of those calculated for benchmark molecular n-type semiconductors such as perylene tetracarbox-ylic diimides (250−322 meV).[73] As shown in Figure 5, the transfer integrals for electron (t_e) and hole (t_h) transports in **D(Ph$_F$CO)-BTBT** and **C$_8$-BTBT** herringbone packings, respectively, are compared along various crystal directions. The corresponding data are collected in Tables S3 and S4. In agreement with the reported values,[74] the largest transfer integrals for **C$_8$-BTBT** are obtained between π-stacked molecules along the crystallographic a-axis (39 meV), whereas smaller values (7 meV) are found between face-to-edge dimers. On the other hand, larger transfer integral values are calculated for **D(Ph$_F$CO)-BTBT** along both the π-stacking (47 meV) and face-to-edge (17 meV) directions. Despite the less pronounced sulfur contributions in **D(Ph$_F$CO)-BTBT**'s LUMO as compared to **C$_8$-BTBT**'s HOMO (Figure S3), LUMO wave function extension through in-plane carbonyl groups appears to play a key role facilitating intermolecular wave function overlaps in the new molecule. Because moderately larger reorganization energy is compensated by larger transfer integrals in the electronic structure of the new molecule, we note that similar charge transport properties could be rationally expected for **D(Ph$_F$CO)-BTBT** and **C$_8$-BTBT**. Furthermore, because a more pronounced 2D charge transport character is expected in **D(Ph$_F$CO)-BTBT**, thermal fluctuations and crystal orientations in the semiconducting channel would have a more limited impact when compared with the reference system of **C$_8$-BTBT**.

■ **CONCLUSIONS**

In summary, the first example of a BTBT-based n-type molecular semiconductor, **D(Ph$_F$CO)-BTBT**, has been designed, synthesized, and characterized. The new semi-conductor was synthesized in a two-step transition-metal-free process without using chromatographic purification. The significant lowering of the LUMO level for **D(Ph$_F$CO)-BTBT**, versus other BTBTs, is attributed to extended π-conjugation along the molecular backbone including the BTBT and in-plane carbonyl units, and, to a less extent, the inductive effect of the out-of-plane pentafluorophenyl groups. Poly-crystalline **D(Ph$_F$CO)-BTBT** thin films exhibit large grains (∼2−5 μm sizes) with "layer-by-layer" packing motifs on the substrate surface forming an in-plane herringbone packing with short intermolecular distances (3.25−3.46 Å), which doubtless favors the 2D source-to-drain (S → D) charge transport. TC/BG-OFET devices comprising a thermally evaporated **D-(Ph$_F$CO)-BTBT** film on the hydrophobic HMDS-treated SiO$_2$ substrate and LiF/Au contacts exhibit high electron mobilities of ∼0.6 cm^2/V s and I_{on}/I_{off}'s over 10^7. The observed high electron mobility for **D(Ph$_F$CO)-BTBT** undoubtedly reflects a combination of a highly π-delocalized/energetically stabilized LUMO, large film grain sizes with high crystallinity, and excellent texture with preferential edge-on molecular orienta-tion and in-plane herringbone packing facilitating strong intermolecular π-orbital overlaps, as supported by DFT computations. Our results demonstrate that n-type semi-conductors based on BTBT cores are possible which, based on the very large intrinsic charge transport capabilities of BTBT (>10 cm^2/V·s) and its good optical transparency, may open new pathways to realize unconventional devices for next-generation high-performance organic (opto)electronics.

■ **ASSOCIATED CONTENT**

ⓈSupporting Information

The Supporting Information is available free of charge on the ACS Publications website at DOI: 10.1021/acs.chemmater.9b01614.

> Chemical characterizations (^{1}H NMR/MALDI TOF-MS spectra) for **D(Ph$_F$CO)-BTBT**, theoretical (DFT/B3LYP/6-31G**) HOMO/LUMO energy levels, and topographical orbital representations; TGA/DSC curves for **D(Ph$_F$CO)-BTBT**, optical absorption/transmission spectra for **D(Ph$_F$CO)-BTBT** film, and optical absorption spectra **D(C$_7$CO)-BTBT**; cyclic voltammo-grams for **C$_8$-BTBT** and **D(C$_7$CO)-BTBT**; single-crystal structure data for **D(Ph$_F$CO)-BTBT**, AFM/2D-GIXD data for **D(Ph$_F$CO)-BTBT** films deposited at 25, 70, 100, and 120 °C; representative transfer/output plots for OFETs fabricated at various conditions and with Ag source−drain electrodes; and tables showing OFET device characteristics and DFT-calculated trans-fer integrals (PDF)

> Crystallographic data of *D(Ph$_F$CO)-BTBT* (CIF)

> Crystallographic data of *D(Ph$_F$CO)-BTBT* (PDF)

■ **AUTHOR INFORMATION**

Corresponding Authors
*E-mail: hakan.usta@agu.edu.tr (H.U.).
*E-mail: afacchetti@flexterracorp.com (A.F.).
*E-mail: myunggil@cau.ac.kr (M.-G.K.).

ORCID

Hakan Usta: 0000-0002-0618-1979
Resul Ozdemir: 0000-0002-7957-110X
M. Carmen Ruiz Delgado: 0000-0001-8180-7153
Gökhan Demirel: 0000-0002-9778-917X
Kilwon Cho: 0000-0003-0321-3629
Antonio Facchetti: 0000-0002-8175-7958

Notes

The authors declare no competing financial interest.

■ REFERENCES

(1) Mei, J.; Diao, Y.; Appleton, A. L.; Fang, L.; Bao, Z. Integrated Materials Design of Organic Semiconductors for Field-Effect Transistors. *J. Am. Chem. Soc.* **2013**, *135*, 6724−6746.

(2) Ozdemir, R.; Choi, D.; Ozdemir, M.; Kwon, G.; Kim, H.; Sen, U.; Kim, C.; Usta, H. Ultralow Bandgap Molecular Semiconductors for Ambient-Stable and Solution-Processable Ambipolar Organic Field-Effect Transistors and Inverters. *J. Mater. Chem. C* **2017**, *5*, 2368−2379.

(3) Yilmaz, M.; Ozdemir, M.; Erdogan, H.; Tamer, U.; Sen, U.; Facchetti, A.; Usta, H.; Demirel, G. Micro-/Nanostructured Highly Crystalline Organic Semiconductor Films for Surface-Enhanced Raman Spectroscopy Applications. *Adv. Funct. Mater.* **2015**, *25*, 5669−5676.

(4) Burnett, E. K.; Ly, J.; Niazi, M. R.; Zhang, L.; McCuskey, S. R.; Amassian, A.; Smilgies, D.-M.; Mannsfeld, S. C. B.; Briseno, A. L. Bistetracene Thin Film Polymorphic Control to Unravel the Effect of Molecular Packing on Charge Transport. *Adv. Mater. Interfaces* **2018**, *5*, 1701607.

(5) Demirel, G.; Usta, H.; Yilmaz, M.; Celik, M.; Alidagi, H. A.; Buyukserin, F. Surface-Enhanced Raman Spectroscopy (SERS): An Adventure from Plasmonic Metals to Organic Semiconductors as SERS Platforms. *J. Mater. Chem. C* **2018**, *6*, 5314−5335.

(6) Figà, V.; Chiappara, C.; Ferrante, F.; Casaletto, M. P.; Principato, F.; Cataldo, S.; Chen, Z.; Usta, H.; Facchetti, A.; Pignataro, B. Symmetric Naphthalenediimidequaterthiophenes for Electropolymerized Electrochromic Thin Films. *J. Mater. Chem. C* **2015**, *3*, 5985−5994.

(7) Kim, M.-G.; Kanatzidis, M. G.; Facchetti, A.; Marks, T. J. Low-Temperature Fabrication of High-Performance Metal Oxide Thin-Film Electronics via Combustion Processing. *Nat. Mater.* **2011**, *10*, 382−388.

(8) Zhang, L.; Colella, N. S.; Cherniawski, B. P.; Mannsfeld, S. C. B.; Briseno, A. L. Oligothiophene Semiconductors: Synthesis, Characterization, and Applications for Organic Devices. *ACS Appl. Mater. Interfaces* **2014**, *6*, 5327−5343.

(9) Liu, Y.; Zhang, L.; Lee, H.; Wang, H. W.; Santala, A.; Liu, F.; Diao, Y.; Briseno, A. L.; Russell, T. P. NDI-Based Small Molecule as Promising Nonfullerene Acceptor for Solution-Processed Organic Photovoltaics. *Adv. Energy Mater.* **2015**, *5*, 1500195.

(10) Kim, J.-O.; Kwon, S. Y.; Kim, Y.; Choi, H. B.; Yang, J. C.; Oh, J.; Lee, H. S.; Sim, J. Y.; Ryu, S.; Park, S. Highly Ordered 3D Microstructure-Based Electronic Skin Capable of Differentiating Pressure, Temperature, and Proximity. *ACS Appl. Mater. Interfaces* **2019**, *11*, 1503−1511.

(11) Ozdemir, M.; Choi, D.; Kwon, G.; Zorlu, Y.; Kim, H.; Kim, M.-G.; Seo, S.; Sen, U.; Citir, M.; Kim, C.; Usta, H. Design, synthesis, and characterization of α,ω-disubstituted indeno[1,2-b]fluorene-6,12-dione-thiophene molecular semiconductors. Enhancement of ambipolar charge transport through synthetic tailoring of alkyl substituents. *RSC Adv.* **2016**, *6*, 212−226.

(12) Son, S. Y.; Lee, G.-Y.; Kim, S.; Park, W.-T.; Park, S. A.; Noh, Y.-Y.; Park, T. Control of Crystallite Orientation in Diketopyrrolopyrrole-Based Semiconducting Polymers via Tuning of Intermolecular Interactions. *ACS Appl. Mater. Interfaces* **2019**, *11*, 10751−10757.

(13) Nketia-yawson, B.; Jung, A.-R.; Nguyen, H. D.; Lee, K.-K.; Kim, B.; Noh, Y.-Y. Difluorobenzothiadiazole and Selenophene-Based Conjugated Polymer Demonstrating an Effective Hole Mobility Exceeding 5 cm2 V-1 s-1 with Solid-State Electrolyte Dielectric. *ACS Appl. Mater. Interfaces* **2018**, *10*, 32492−32500.

(14) Kim, J.-O.; Lee, J. C.; Kim, M. J.; Noh, H.; Yeom, H. I.; Ko, J. B.; Lee, T. H.; Ko Park, S. H.; Kim, D. P.; Park, S. Inorganic Polymer Micropillar-Based Solution Shearing of Large-Area Organic Semiconductor Thin Films with Pillar-Size-Dependent Crystal Size. *Adv. Mater.* **2018**, *30*, 1870216.

(15) Shi, S.; Wang, H.; Uddin, M. A.; Yang, K.; Su, M.; Bianchi, L.; Chen, P.; Cheng, X.; Guo, H.; Zhang, S.; Woo, H. Y.; Guo, X. Head-to-Head Linked Dialkylbifuran-Based Polymer Semiconductors for High-Performance Organic Thin-Film Transistors with Tunable Charge Carrier Polarity. *Chem. Mater.* **2019**, *31*, 1808−1817.

(16) Shi, Y.; Guo, H.; Qin, M.; Wang, Y.; Zhao, J.; Sun, H.; Wang, H.; Wang, Y.; Zhou, X.; Facchetti, A.; Lu, X.; Zhou, M.; Guo, X. Imide-Functionalized Thiazole-Based Polymer Semiconductors: Synthesis, Structure-Property Correlations, Charge Carrier Polarity, and Thin-Film Transistor Performance. *Chem. Mater.* **2018**, *30*, 7988−8001.

(17) Horowitz, G.; Fichou, D.; Peng, X.; Garnier, F. Thin-Film Transistors Based on Alpha-Conjugated Oligomers. *Synth. Met.* **1991**, *41*, 1127−1130.

(18) Anthony, J. E. Functionalized Acenes and Heteroacenes for Organic Electronics. *Chem. Rev.* **2006**, *106*, 5028−5048.

(19) Facchetti, A. Semiconductors for Organic Transistors. *Mater. Today* **2007**, *10*, 28−37.

(20) Niimi, K.; Shinamura, S.; Osaka, I.; Miyazaki, E.; Takimiya, K. Dianthra[2,3-b:2′,3′-f]thieno[3,2-b]thiophene (DATT): Synthesis, Characterization, and FET Characteristics of New π-Extended Heteroarene with Eight Fused Aromatic Rings. *J. Am. Chem. Soc.* **2011**, *133*, 8732−8739.

(21) Horton, A. W. The Mechanism of the Reactions of Hydrocarbons with Sulfur1. *J. Org. Chem.* **1949**, *14*, 761−770.

(22) Kaszynski, P.; Dougherty, D. A. Synthesis and Properties of Diethyl 5,10-Dihetera-5,10-Dihydroindeno[2,1-a]Indene-2,7-Dicarboxylates. *J. Org. Chem.* **1993**, *58*, 5209−5220.

(23) Košata, B.; Kozmik, V.; Svoboda, J.; Novotná, V.; Vaněk, P.; Glogarová, M. Novel Liquid Crystals Based on [1]Benzothieno[3,2-b][1]Benzothiophene. *Liq. Cryst.* **2003**, *30*, 603−610.

(24) Takimiya, K.; Ebata, H.; Sakamoto, K.; Izawa, T.; Otsubo, T.; Kunugi, Y. 2,7-Diphenyl[1]benzothieno[3,2-b]benzothiophene, A New Organic Semiconductor for Air-Stable Organic Field-Effect Transistors with Mobilities up to 2.0 cm2V-1s-1. *J. Am. Chem. Soc.* **2006**, *128*, 12604−12605.

(25) Ebata, H.; Izawa, T.; Miyazaki, E.; Takimiya, K.; Ikeda, M.; Kuwabara, H.; Yui, T. Highly Soluble [1]Benzothieno[3,2-b]-Benzothiophene (BTBT) Derivatives for High-Performance, Solution-Processed Organic Field-Effect Transistors. *J. Am. Chem. Soc.* **2007**, *129*, 15732−15733.

(26) Um, M.-C.; Kwak, J.; Hong, J.-P.; Kang, J.; Yoon, D. Y.; Lee, S. H.; Lee, C.; Hong, J.-I. High-Performance Organic Semiconductors for Thin-Film Transistors Based on 2,7-Divinyl[1]Benzothieno[3,2-b]Benzothiophene. *J. Mater. Chem.* **2008**, *18*, 4698−4703.

(27) Amin, A. Y.; Khassanov, A.; Reuter, K.; Meyer-Friedrichsen, T.; Halik, M. Low-Voltage Organic Field Effect Transistors with a 2-

Tridecyl[1]benzothieno[3,2-b][1]benzothiophene Semiconductor Layer. *J. Am. Chem. Soc.* **2012**, *134*, 16548−16550.

(28) Iino, H.; Usui, T.; Hanna, J.-I. Liquid Crystals for Organic Thin-Film Transistors. *Nat. Commun.* **2015**, *6*, 6828.

(29) He, Y.; Xu, W.; Murtaza, I.; Zhang, D.; He, C.; Zhu, Y.; Meng, H. Molecular phase engineering of organic semiconductors based on a [1]benzothieno[3,2-b][1]benzothiophene core. *RSC Adv.* **2016**, *6*, 95149−95155.

(30) Schweicher, G.; Lemaur, V.; Niebel, C.; Ruzié, C.; Diao, Y.; Goto, O.; Lee, W. Y.; Kim, Y.; Arlin, J. B.; Karpinska, J.; Kennedy, A. R.; Parkin, S. R.; Olivier, Y.; Mannsfeld, S. C. B.; Cornil, J.; Geerts, Y. H.; Bao, Z. Bulky End-Capped [1]Benzothieno[3,2- b]-benzothiophenes: Reaching High-Mobility Organic Semiconductors by Fine Tuning of the Crystalline Solid-State Order. *Adv. Mater.* **2015**, *27*, 3066−3072.

(31) He, Y.; Sezen, M.; Zhang, D.; Li, A.; Yan, L.; Yu, H.; He, C.; Goto, O.; Loo, Y.-L.; Meng, H. High Performance OTFTs Fabricated Using a Calamitic Liquid Crystalline Material of 2-(4-Dodecyl phenyl)[1]benzothieno[3,2-b][1]benzothiophene. *Adv. Electron. Mater.* **2016**, *2*, 1600179.

(32) He, K.; Li, W.; Tian, H.; Zhang, J.; Yan, D.; Geng, Y.; Wang, F. Asymmetric Conjugated Molecules Based on [1]Benzothieno[3,2-b][1]Benzothiophene for High-Mobility Organic Thin-Film Transistors: Influence of Alkyl Chain Length. *ACS Appl. Mater. Interfaces* **2017**, *9*, 35427−35436.

(33) Reddy, M. R.; Kim, H.; Kim, C.; Seo, S. 2-Thiophene[1]-Benzothieno[3,2- b]Benzothiophene Derivatives as Solution-Processable Organic Semiconductors for Organic Thin-Film Transistors. *Synth. Met.* **2018**, *235*, 153−159.

(34) Yuan, Y.; Giri, G.; Ayzner, A. L.; Zoombelt, A. P.; Mannsfeld, S. C. B.; Chen, J.; Nordlund, D.; Toney, M. F.; Huang, J.; Bao, Z. Ultra-High Mobility Transparent Organic Thin Film Transistors Grown by an off-Centre Spin-Coating Method. *Nat. Commun.* **2014**, *5*, 3005.

(35) Minemawari, H.; Yamada, T.; Matsui, H.; Tsutsumi, J. Y.; Haas, S.; Chiba, R.; Kumai, R.; Hasegawa, T. Inkjet Printing of Single-Crystal Films. *Nature* **2011**, *475*, 364−367.

(36) Takimiya, K.; Shinamura, S.; Osaka, I.; Miyazaki, E. Thienoacene-Based Organic Semiconductors. *Adv. Mater.* **2011**, *23*, 4347−4370.

(37) Mori, T.; Nishimura, T.; Yamamoto, T.; Doi, I.; Miyazaki, E.; Osaka, I.; Takimiya, K. Consecutive Thiophene-Annulation Approach to π-Extended Thienoacene-Based Organic Semiconductors with [1]Benzothieno[3,2-b][1]benzothiophene (BTBT) Substructure. *J. Am. Chem. Soc.* **2013**, *135*, 13900−13913.

(38) Takimiya, K.; Yamamoto, T.; Ebata, H.; Izawa, T. Design Strategy for Air-Stable Organic Semiconductors Applicable to High-Performance Field-Effect Transistors. *Sci. Technol. Adv. Mater.* **2007**, *8*, 273−276.

(39) Facchetti, A.; Mushrush, M.; Yoon, M.-H.; Hutchison, G. R.; Ratner, M. A.; Marks, T. J. Building Blocks for n-Type Molecular and Polymeric Electronics. Perfluoroalkyl- versus Alkyl-Functionalized Oligothiophenes (nT;n= 2−6). Systematics of Thin Film Microstructure, Semiconductor Performance, and Modeling of Majority Charge Injection in Field-Effect Transistors. *J. Am. Chem. Soc.* **2004**, *126*, 13859−13874.

(40) Facchetti, A.; Yoon, M.-H.; Stern, C. L.; Hutchison, G. R.; Ratner, M. A.; Marks, T. J. Building Blocks for N-Type Molecular and Polymeric Electronics. Perfluoroalkyl- versus Alkyl-Functionalized Oligothiophenes (nTs;n= 2−6). Systematic Synthesis, Spectroscopy, Electrochemistry, and Solid-State Organization. *J. Am. Chem. Soc.* **2004**, *126*, 13480−13501.

(41) Facchetti, A.; Letizia, J.; Yoon, M.-H.; Mushrush, M.; Katz, H. E.; Marks, T. J. Synthesis and Characterization of Diperfluorooctyl-Substituted Phenylene−Thiophene Oligomers as n-Type Semiconductors. Molecular Structure−Film Microstructure−Mobility Relationships, Organic Field-Effect Transistors, and Transistor Nonvolatile Memory Elements. *Chem. Mater.* **2004**, *16*, 4715−4727.

(42) Tsutsumi, J.; Matsuoka, S.; Inoue, S.; Minemawari, H.; Yamada, T.; Hasegawa, T. N-Type Field-Effect Transistors Based on Layered

Crystalline Donor-Acceptor Semiconductors with Dialkylated Benzo-thienobenzothiophenes as Electron Donors. *J. Mater. Chem. C* **2015**, *3*, 1976−1981.

(43) Tang, M. L.; Bao, Z. Halogenated Materials as Organic Semiconductors. *Chem. Mater.* **2011**, *23*, 446−455.

(44) Letizia, J. A.; Facchetti, A.; Stern, C. L.; Ratner, M. A.; Marks, T. J. High Electron Mobility in Solution-Cast and Vapor-Deposited Phenacyl−Quaterthiophene-Based Field-Effect Transistors: Toward N-Type Polythiophenes. *J. Am. Chem. Soc.* **2005**, *127*, 13476−13477.

(45) Frisch, M. J.; Trucks, G. W.; Schlegel, H. B.; Scuseria, G. E.; Robb, M. A.; Cheeseman, J. R.; Scalmani, G.; Barone, V.; Mennucci, B.; Petersson, G. A.; Nakatsuji, H.; Caricato, M.; Li, X.; Hratchian, H. P.; Izmaylov, A. F.; Bloino, J.; Zheng, G.; Sonnenberg, J. L.; Hada, M.; Ehara, M.; Toyota, K.; Fukuda, R.; Hasegawa, J.; Ishida, M.; Nakajima, T.; Honda, Y.; Kitao, O.; Nakai, H.; Vreven, T.; Montgomery, J. A., Jr.; Peralta, J. E.; Ogliaro, F.; Bearpark, M.; Heyd, J. J.; Brothers, E.; Kudin, K. N.; Staroverov, V. N.; Keith, T.; Kobayashi, R.; Normand, J.; Raghavachari, K.; Rendell, A.; Burant, J. C.; Iyengar, S. S.; Tomasi, J.; Cossi, M.; Rega, N.; Millam, J. M.; Klene, M.; Knox, J. E.; Cross, J. B.; Bakken, V.; Adamo, C.; Jaramillo, J.; Gomperts, R.; Stratmann, R. E.; Yazyev, O.; Austin, A. J.; Cammi, R.; Pomelli, C.; Ochterski, J. W.; Martin, R. L.; Morokuma, K.; Zakrzewski, V. G.; Voth, G. A.; Salvador, P.; Dannenberg, J. J.; Dapprich, S.; Daniels, A. D.; Farkas, O.; Foresman, J. B.; Ortiz, J. V.; Cioslowski, J.; Fox, D. J. *Gaussian 09*, Revision C.01, 2010; Gaussian, Inc.: Wallingford, CT.

(46) Brédas, J.-L.; Beljonne, D.; Coropceanu, V.; Cornil, J. Charge-Transfer and Energy-Transfer Processes in π-Conjugated Oligomers and Polymers: A Molecular Picture. *Chem. Rev.* **2004**, *104*, 4971−5004.

(47) Valeev, E. F.; Coropceanu, V.; da Silva Filho, D. A.; Salman, S.; Brédas, J.-L. Effect of Electronic Polarization on Charge-Transport Parameters in Molecular Organic Semiconductors. *J. Am. Chem. Soc.* **2006**, *128*, 9882−9886.

(48) Becke, A. D. Density-functional thermochemistry. III. The role of exact exchange. *J. Chem. Phys.* **1993**, *98*, 5648−5652.

(49) Lee, C.; Yang, W.; Parr, R. G. Development of the Colle-Salvetti Correlation-Energy Formula into a Functional of the Electron Density. *Phys. Rev. B: Condens. Matter Mater. Phys.* **1988**, *37*, 785−789.

(50) Perdew, J. P.; Chevary, J. A.; Vosko, S. H.; Jackson, K. A.; Pederson, M. R.; Singh, D. J.; Fiolhais, C. Atoms, Molecules, Solids and Surfaces: Applications of the GGA for Exchange Correlation. *Phys. Rev. B: Condens. Matter Mater. Phys.* **1992**, *46*, 6671−6687.

(51) Perdew, J. P.; Chevary, J. A.; Vosko, S. H.; Jackson, K. A.; Pederson, M. R.; Singh, D. J.; Fiolhais, C. Erratum: Atoms, Molecules, Solids, and Surfaces: Applications of the Generalized Gradient Approximation for Exchange and Correlation. *Phys. Rev. B: Condens. Matter Mater. Phys.* **1993**, *48*, 4978.

(52) Hehre, W. J.; Ditchfield, R.; Pople, J. A. Self-Consistent Molecular Orbital Methods. XII. Further Extensions of Gaussian-Type Basis Sets for Use in Molecular Orbital Studies of Organic Molecules. *J. Chem. Phys.* **1972**, *56*, 2257−2261.

(53) Francl, M. M.; Pietro, W. J.; Hehre, W. J.; Binkley, J. S.; Gordon, M. S.; DeFrees, D. J.; Pople, J. A. Self-consistent Molecular Orbital Methods. XXIII. A Polarization-type Basis Set for Second-row Elements. *J. Chem. Phys.* **1982**, *77*, 3654−3665.

(54) Sini, G.; Sears, J. S.; Brédas, J.-L. Evaluating the Performance of DFT Functionals in Assessing the Interaction Energy and Ground-State Charge Transfer of Donor/Acceptor Complexes: Tetrathiaful-valene-Tetracyanoquinodimethane (TTF-TCNQ) as a Model Case. *J. Chem. Theory Comput.* **2011**, *7*, 602−609.

(55) Chen, M.-C.; Chiang, Y.-J.; Kim, C.; Guo, Y.-J.; Chen, S.-Y.; Liang, Y.-J.; Huang, Y.-W.; Hu, T.-S.; Lee, G.-H.; Facchetti, A.; Marks, T. J. One-Pot [1+1+1] Synthesis of Dithieno[2,3-b:3′,2′-d]-Thiophene (DTT) and Their Functionalized Derivatives for Organic Thin-Film Transistors. *Chem. Commun.* **2009**, 1846−1848.

(56) Schwarzer, A.; Seichter, W.; Weber, E.; Stoeckli-Evans, H.; Losada, M.; Hulliger, J. Supramolecular Control of Fluorinated

Benzophenones in the Crystalline State. *CrystEngComm* **2004**, *6*, 567−572.

(57) Yoon, M.-H.; Facchetti, A.; Stern, C. E.; Marks, T. J. Fluorocarbon-Modified Organic Semiconductors: Molecular Architecture, Electronic, and Crystal Structure Tuning of Arene- versus Fluoroarene-Thiophene Oligomer Thin-Film Properties. *J. Am. Chem. Soc.* **2006**, *128*, 5792−5801.

(58) Wang, C.; Dong, H.; Hu, W.; Liu, Y.; Zhu, D. Semiconducting π-Conjugated Systems in Field-Effect Transistors: A Material Odyssey of Organic Electronics. *Chem. Rev.* **2012**, *112*, 2208−2267.

(59) Usta, H.; Facchetti, A. Organic Semiconductors for Transparent Electronics. *Flexible Carbon-Based Electronics*; Wiley-VCH Verlag GmbH & Co. KGaA: Weinheim, Germany, 2018; pp 13−50.

(60) Capelli, R.; Toffanin, S.; Generali, G.; Usta, H.; Facchetti, A.; Muccini, M. Organic Light-Emitting Transistors with an Efficiency That Outperforms the Equivalent Light-Emitting Diodes. *Nat. Mater.* **2010**, *9*, 496−503.

(61) Katz, H. E.; Johnson, J.; Lovinger, A. J.; Li, W. Naphthalenetetracarboxylic Diimide-Based n-Channel Transistor Semiconductors: Structural Variation and Thiol-Enhanced Gold Contacts. *J. Am. Chem. Soc.* **2000**, *122*, 7787−7792.

(62) Jones, B. A.; Facchetti, A.; Wasielewski, M. R.; Marks, T. J. Tuning Orbital Energetics in Arylene Diimide Semiconductors. Materials Design for Ambient Stability of n-Type Charge Transport. *J. Am. Chem. Soc.* **2007**, *129*, 15259−15278.

(63) Yagi, I.; Tsukagoshi, K.; Aoyagi, Y. Modification of the Electric Conduction at the Pentacene SiO2 Interface by Surface Termination of SiO2. *Appl. Phys. Lett.* **2005**, *86*, 103502.

(64) Yang, H.; Shin, T. J.; Ling, M.-M.; Cho, K.; Ryu, C. Y.; Bao, Z. Conducting AFM and 2D GIXD Studies on Pentacene Thin Films. *J. Am. Chem. Soc.* **2005**, *127*, 11542−11543.

(65) Chu, C.-W.; Li, S.-H.; Chen, C.-W.; Shrotriya, V.; Yang, Y. High-Performance Organic Thin-Film Transistors with Metal Oxide/ Metal Bilayer Electrode. *Appl. Phys. Lett.* **2005**, *87*, 193508.

(66) Zhou, Y.; Fuentes-Hernandez, C.; Shim, J.; Meyer, J.; Giordano, A. J.; Li, H.; Winget, P.; Papadopoulos, T.; Cheun, H.; Kim, J.; Fenoll, M.; Dindar, A.; Haske, W.; Najafabadi, E.; Khan, T. M.; Sojoudi, H.; Barlow, S.; Graham, S.; Bredas, J.-L.; Marder, S. R.; Kahn, A.; Kippelen, B. A Universal Method to Produce Low-Work Function Electrodes for Organic Electronics. *Science* **2012**, *336*, 327−332.

(67) Liu, C.; Xu, Y.; Noh, Y.-Y. Contact Engineering in Organic Field-Effect Transistors. *Mater. Today* **2015**, *18*, 79−96.

(68) Sun, Z.; Shi, S.; Bao, Q.; Liu, X.; Fahlman, M. Role of Thick-Lithium Fluoride Layer in Energy Level Alignment at Organic/Metal Interface: Unifying Effect on High Metallic Work Functions. *Adv. Mater. Interfaces* **2015**, *2*, 1400527.

(69) Usta, H.; Facchetti, A.; Marks, T. J. N -Channel Semiconductor Materials Design for Organic Complementary Circuits. *Acc. Chem. Res.* **2011**, *44*, 501−510.

(70) Yan, Z.; Sun, B.; Li, Y. Novel Stable (3E,7E)-3,7-Bis(2-Oxoindolin-3-Ylidene)Benzo[1,2-b:4,5-B′]Difuran-2,6(3H,7H)-Dione Based Donor-Acceptor Polymer Semiconductors for n-Type Organic Thin Film Transistors. *Chem. Commun.* **2013**, *49*, 3790−3792.

(71) Huang, J.; Mao, Z.; Chen, Z.; Gao, D.; Wei, C.; Zhang, W.; Yu, G. Diazaisoindigo-Based Polymers with High-Performance Charge-Transport Properties: From Computational Screening to Experimental Characterization. *Chem. Mater.* **2016**, *28*, 2209−2218.

(72) Usta, H.; Sheets, W. C.; Denti, M.; Generali, G.; Capelli, R.; Lu, S.; Yu, X.; Muccini, M.; Facchetti, A. Perfluoroalkyl-Functionalized Thiazole-Thiophene Oligomers as N-Channel Semiconductors in Organic Field-Effect and Light-Emitting Transistors. *Chem. Mater.* **2014**, *26*, 6542−6556.

(73) Delgado, M. C. R.; Kim, E.-G.; Filho, D. A.; Bredas, J.-L. Tuning the Charge-Transport Parameters of Perylene Diimide Single Crystals via End and/or Core Functionalization: A Density Functional Theory Investigation. *J. Am. Chem. Soc.* **2010**, *132*, 3375−3387.

(74) Nan, G.; Li, Z. Crystal Structure versus Charge Transport in Organic Single Crystals of [1]Benzothieno[3,2-b][1]Benzothiophene Derivatives from a Multiscale Theoretical Study. *J. Mater. Chem. C* **2014**, *2*, 1447−1456.